



Improved exfoliation of surface-functionalized graphene oxide by epoxy monomer and enhanced mechanical properties of epoxy nanocomposites

Jie Fan¹, Jiping Yang^{1,*} , Hong Li², Junpeng Tian¹, Jinrui Ye³, and Yunfeng Zhao^{1,4,*}

¹Key Laboratory of Aerospace Advanced Materials and Performance, Ministry of Education, School of Materials Science and Engineering, Beihang University, Beijing 100191, China

²713Th Research Institute of China Shipbuilding Industry Corporation, Henan 450015, China

³Association for Science and Technology, Beihang University, Beijing 100191, China

⁴Aerospace Research Institute of Materials and Processing Technology, Beijing 100076, China

Received: 17 March 2021

Accepted: 29 September 2021

Published online:

11 October 2021

© The Author(s), under exclusive licence to Springer Science+Business Media, LLC, part of Springer Nature 2021

ABSTRACT

The surface functionalization of graphene oxide (GO) provides an efficient way to improve the dispersion of GO in matrix and the interfacial properties of nanocomposites. In this contribution, GO grafted by bifunctional, trifunctional and tetrafunctional epoxy monomers (E51, AFG90, AG80) was designed and three epoxy-functionalized GO (EFGO) samples were acquired and utilized as fillers for epoxy nanocomposites. The chemical, structural and morphological characteristics of EFGO samples were studied. The exfoliation and dispersion state of EFGO in epoxy matrix were characterized. Mechanical properties of the nanocomposites at room temperature (RT), liquid nitrogen temperature (LNT) and after thermal cycling were comprehensively investigated. Results showed that the interlayer distance of EFGO was enlarged with the increase in functionality degree of the grafted epoxy monomers. AG80-functionalized GO (AGGO) with the largest interlayer distance showed the best exfoliation and dispersion in the nanocomposites, while E51-functionalized GO (EGO) showed the worst. Correspondingly, AGGO/epoxy nanocomposites exhibited the highest mechanical properties at RT, LNT and after thermal cycling. The toughening mechanisms of EFGO for epoxy resin were disclosed to better understand the role of epoxy monomers grafted to GO surfaces in the nanocomposites.

Handling Editor: Chris Cornelius.

Address correspondence to E-mail: jyang@buaa.edu.cn; zhaoyf703@163.com

Introduction

Graphene, renowned for its unparalleled mechanical properties (Young's modulus of 1 TPa, tensile strength of 130 GPa [1]), outstanding carrier mobility and thermal conductivity [2, 3], has been widely applied in electronics, biomedicine, aerospace and other fields [4, 5]. To make use of its mechanical properties, graphene has been introduced into polymers aiming to fabricate high-performance nanocomposites [6–8]. However, graphene sheets tend to form aggregation in the matrix due to the strong van der Waals interactions between the sheets and the inferior compatibility with polymers [9, 10], causing great limitation to their application. Comparatively, graphene oxide (GO) can not only ameliorate the aggregation of graphene in the polymer [11], but also provide reactive sites for further functionalization due to the abundant oxygen-containing functional groups on surfaces [12] and therefore becomes a perfect substitute.

Considerable research has reported that GO and its derivatives can improve the strength and toughness of nanocomposites [13, 14]. The reinforcing efficiency is crucially determined by the dispersion of fillers and the interface between fillers and the matrix [15, 16]. Through interfacial design achieved by GO functionalization, the interfacial characteristics can be effectively modulated. Chemical amidation and carboxylation of GO are widely used functionalization methods [17–19]. As for the most widely applied epoxy resin [20–23], grafting epoxy monomers onto GO surfaces provide another insight for preparing high-performance epoxy nanocomposites [24, 25]. The epoxy chains grafted to GO surfaces can improve the compatibility of GO with epoxy resin and create a possibility for the cross-linking between GO and epoxy matrix, leading to strong interfacial bonds and powerful stress transfer. The effectiveness of epoxy functionalization in improving the dispersion of epoxy-functionalized GO (EFGO) and mechanical properties of EFGO/epoxy nanocomposites has already been reported by Wan et al. [26].

According to the previous research, the rigidity, functionality degree and chain length of the grafted epoxy chains play a significant role in the interfacial characteristics and mechanical properties of EFGO/epoxy nanocomposites [27]. However, GO has been functionalized by only one type of epoxy monomer in

most of the reports. The systematical research is still rare and deserves much attention. Besides, the recent rapid development of aerospace technology accelerates the application of epoxy resin in cryogenic projects at ultra-low temperature and even under thermal cycling conditions [28–30]. Unfortunately, the reported research mainly focuses on the mechanical properties of epoxy nanocomposites at room temperature (RT) [31–33], while those under cryogenic conditions like at liquid nitrogen temperature (LNT) and after thermal cycling are rarely considered.

In the present work, three types of epoxy monomers with varied epoxy functionality degrees (two, three and four) were utilized to covalently functionalize GO and EFGO/epoxy nanocomposites were prepared. The successful functionalization of GO was confirmed by chemical, structural and morphological characterizations. The exfoliation and dispersion state of EFGO in the matrix were compared. The mechanical properties of nanocomposites at RT and LNT as well as after thermal cycling were investigated. The toughening mechanisms of EFGO for epoxy resin at RT and LNT were both disclosed based on the tensile fracture morphology of the nanocomposites.

Experimental

Materials

E51 (a bifunctional epoxy resin), with an epoxide equivalent of 185–190 g·eq⁻¹, Mn (number-average molecular weight) of 392 g·mol⁻¹, viscosity of 14.8 Pa·s at room temperature, was purchased from Nantong Xingchen Synthetic Material Co., Ltd, China. AFG90 (a trifunctional epoxy resin with Mn of 277 g·mol⁻¹ and viscosity of 6.2 Pa·s at room temperature) and AG80 (a tetrafunctional epoxy resin with Mn of 422 g·mol⁻¹ and viscosity of 185.6 Pa·s at room temperature) were obtained from Hubei Zhenzhengfeng New Material Co., Ltd, China. Chemical structures of the three epoxy molecules are shown in Fig. S1. And the chemical analysis including FTIR (Fourier transform infrared spectra), ¹H-NMR (proton nuclear magnetic resonance spectra) and GPC (gel permeation chromatography) results of epoxy monomers can be seen from Supporting Information S2. Imidazole, the curing agent, was

supplied by Shanghai Macklin Biochemical Co., Ltd, China. Natural graphite (99%, 325 mesh) was provided by Qingdao Tengshenda Tansu Jixie Co., Ltd, China. Triphenylphosphine (TPP) was purchased from Innochem Technology Co., Ltd, China. Sulfuric acid (H_2SO_4 , 98%), peroxide (H_2O_2 , 30%), hydrochloric acid (HCl, 37%), and solvents of ethanol, acetone, dimethylformamide (DMF), tetrahydrofuran (THF) were supplied by Beijing Modern Oriental Technology Development Co., Ltd, China. Potassium permanganate (KMnO_4 , 98%) was obtained from Sinopharm Chemical Reagent Co., Ltd. All the reagents were directly used as received.

Preparation of functionalized GO

GO was prepared by a modified Hummer's method according to our previous work [34–36], and the procedure can be seen in Supporting Information S3. The covalent functionalization of GO by epoxy monomers was performed following the steps reported by Shen et al. [25]. To be specific, GO was dispersed in DMF and sonicated for 1 h to achieve a homogenous GO/DMF dispersion (2 mg/ml). Then, 10 ~ 20 g E51, AFG90 or AG80 was dissolved in 20 ml DMF and added into GO/DMF dispersion. The mixture was sonicated for 0.5 h and TPP (0.50 wt% to epoxy) was added as the catalyst. The reaction was kept at 100 °C for 24 h under magnetic stirring. Then, the product was washed with DMF or acetone several times to remove the unreacted epoxy and TPP. EFGO was dried at 50 °C for hours in a vacuum oven. The acquired samples of E51-functionalized GO, AFG90-functionalized GO and AG80-functionalized GO were denoted as EGO, AFGO and AGGO, respectively.

Preparation of epoxy nanocomposites

The nanocomposites were prepared through a solvent mixing method with the help of a three-roll milling technique according to our previous work [36]. EFGO samples were dispersed in the mixed solvents of acetone and ethanol by sonication (2 mg/ml). Then, E51 solution in acetone (1.5–1.6 mg/ml, 0.25 Pa.s at 25 °C) was added and the mixture was magnetically stirred overnight. Most of the solvent was removed by rotary evaporation. After that, the mixture was milled by a three-roll mill to acquire epoxy masterbatch with 0.60 wt% EFGO. The

masterbatch was mixed with E51 and 3.5 phr of imidazole to prepare nanocomposites with EFGO loadings of 0.1 wt%, 0.3 wt% and 0.5 wt%, respectively. The paste was degassed under vacuum and cast into molds and finally cured at 60 °C for 2 h, 80 °C for 1 h, 110 °C for 3 h and 130 °C for 2 h referring to our previous work [36, 37].

Characterizations

FTIR spectra were acquired from a Nicolet 6700 Fourier transform infrared spectrometer using the KBr pellet pressing method or attenuated total reflectance (ATR) method. GPC tests were performed on a Waters 515-717-2410 GPC System using THF as the mobile phase. $^1\text{H-NMR}$ spectra were tested on a Bruker AV400 spectrometer using deuterated trichloromethane as the solvent. Thermogravimetric tests (TGs) of the samples were performed on a Shimadzu TGA-50H thermogravimetric analyzer under nitrogen. The X-ray diffraction (XRD) spectra of the samples from 3° to 35° were taken from a Rigaku Dmax2200 diffractometer using CuK α radiation ($\lambda = 0.15418$ nm). GO sample in a film state as dried from the water solution was used in the test, and its diffraction peak was very strong with high S/N ratio (signal-to-noise ratio). The three EFGO samples were all dried from their ethanol solutions and in powder state for the test. Raman spectra of EFGO powders were tested on a LabRAM HR800 Raman spectrometer using 633-nm laser wavelength. The atomic force microscope (AFM) measurements of EFGO samples were taken on a Bruker ICON atomic force microscope. To prepare samples for AFM tests, a few drops of EFGO solution were placed on the fresh mica surface and dried at room temperature.

To observe the dispersion of EFGO in the matrix, EFGO/epoxy masterbatches were dropped onto the glass slide and covered by a coverslip. Then, the samples were observed by a Carl Zeiss optical microscope. The dispersion of EFGO in the cured nanocomposites was investigated by a JEOLJEM-2100F transmission electron microscope (TEM) using the ultrathin sections cut from the nanocomposites. The morphology study was finished using a JEOL JSM6010 field emission scanning electron microscope (SEM). Samples were fixed onto an aluminum stage using the conductive adhesive films and sputter-coated with gold twice before observation.

Dumbbell-shaped specimens for tensile tests with the length of 115 mm and thickness of 3.2 ± 0.4 mm were prepared according to ASTM D638 [38, 39]. A SANS Electronic Universal Testing Machine (50 KN) was used to perform the tests with the cross-head speed of 1 mm/min at RT and LNT. To achieve the cryogenic conditions, samples were immersed in liquid nitrogen for 10 min and tensile tests were conducted with the fixtures in liquid nitrogen. For the thermal cycling experiments, tensile samples were immersed in liquid nitrogen for 5 min and then stored in the oven at 35 °C for another 5 min. The round was repeated 20 times to simulate the practical thermal cycling environment of some apparatus like cryogenic fuel tanks. After thermal cycling, tensile samples were stored at room temperature for 2 h and then tested at room temperature.

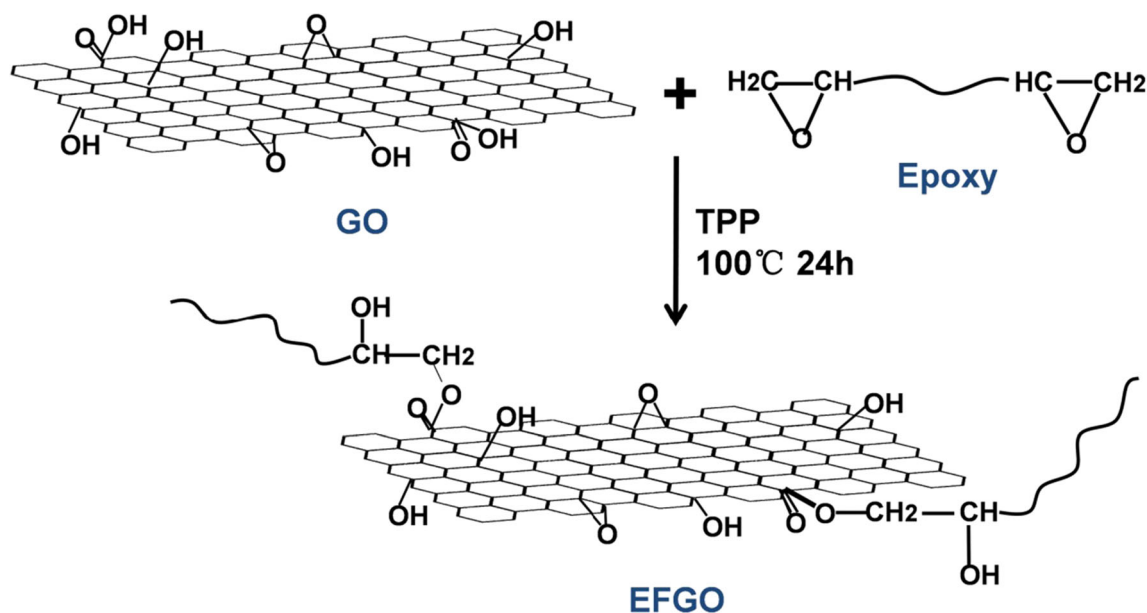
Results and discussion

Characterization of epoxy-functionalized GO

Through the chemical reaction between the oxygen-containing groups on GO surfaces and epoxy groups of epoxy monomers with TPP as the catalyst, the epoxy molecules are grafted to GO surfaces. The functionalization process is shown in Scheme 1 [40, 41].

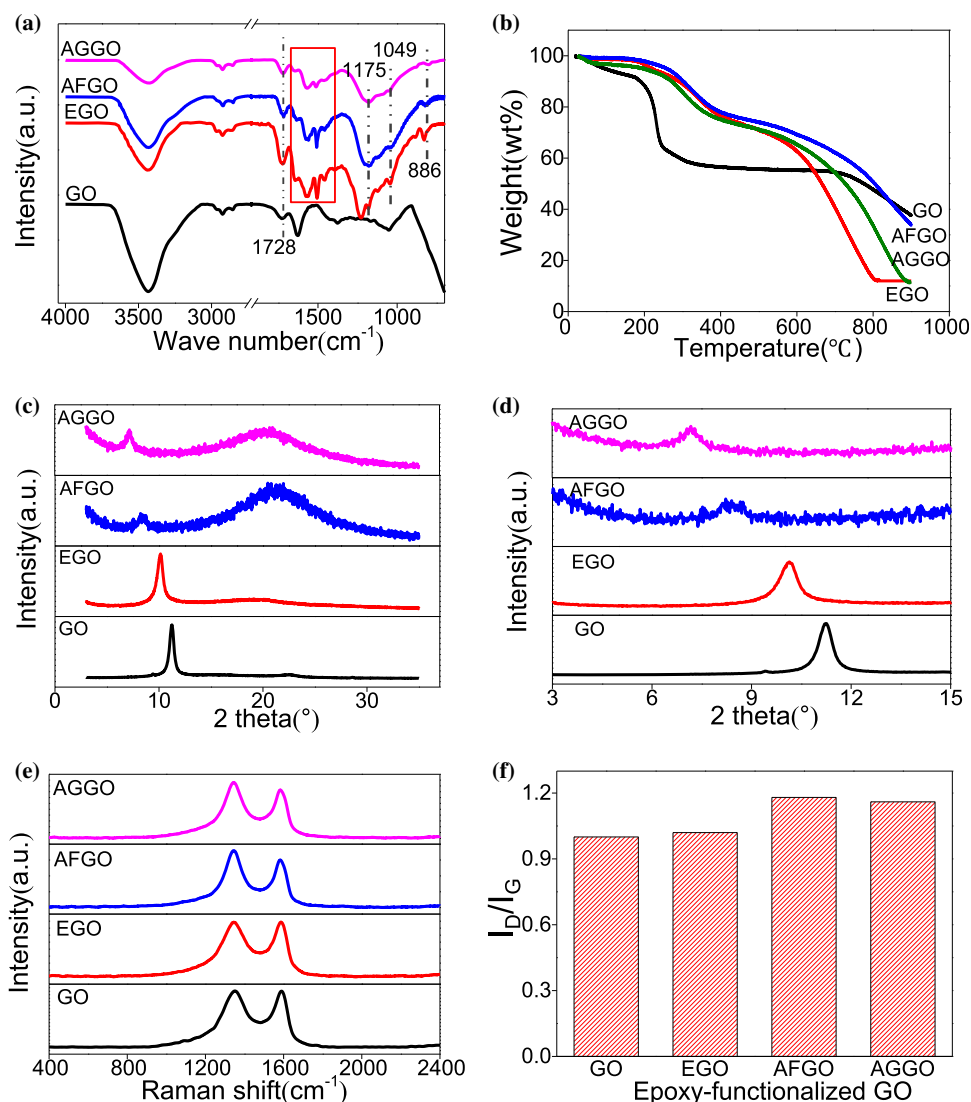
The successful covalent functionalization of GO by varied epoxy monomers is confirmed by FTIR spectra, as shown in Fig. 1a. Peaks at 1728 cm^{-1} and 1630 cm^{-1} are assigned to C = O bonds and C = C bonds [42], respectively, which can be seen in the spectra of GO and all three EFGO samples. New peaks from the vibrations of the benzene ring skeleton appear in the spectra of EFGO samples at $1650 \sim 1450\text{ cm}^{-1}$ (1630 cm^{-1} , 1570 cm^{-1} , 1504 cm^{-1} and 1459 cm^{-1}) [43]. What's important, there is also the characteristic peak of the epoxide group located near 886 cm^{-1} in the spectra of EFGO samples [44]. In addition, peaks at 1175 cm^{-1} and 1049 cm^{-1} are attributed to the stretching vibrations of C–O bonds in ether and benzene ring, respectively [45]. Considering the change from brown GO to black EFGO powders and the rigorous washing process, it is believed that epoxy molecules have been successfully chemically grafted onto GO surfaces.

TG plots were investigated to determine the epoxy grafting density of EFGO samples. It can be observed from Fig. 1b that EFGO samples exhibit higher thermal stability than GO. GO shows a steep weight loss at around 200 °C due to the degradation of oxygen-containing functional groups on its surfaces. EFGO samples have a major weight loss at 310 °C, indicating the decomposition of the grafted epoxy molecules, which is similar to the previously reported results [24]. The weight loss of EFGO after 600 °C is attributed to the breaking of the carbon skeleton. All



Scheme 1 The chemical reaction between GO and epoxy monomers.

Figure 1 FTIR spectra (a), TG plots (b), XRD spectra in 3–35°(c) and 3–15°(d), Raman spectra (e) and the calculated I_D/I_G (f) of GO and EFGO samples.



the EFGO samples show a lower thermal stability than GO after 600 °C, but the decrease extents are different. The grafted E51 molecule with a linear long chain and a high molecular weight may cause more severe damage to the carbon skeleton of GO sample, while AFG90 molecule with the lowest molecular weight causes slighter damage.

The grafting weight percent (G_W) of EFGO is acquired from the weight loss at around 310 °C. And the grafting density (G_D) is calculated according to formula (1) referring to our previous work [46].

$$G_D = \frac{G_W/M_n}{(1 - G_W)/M_C} \quad (1)$$

where M_n is the number-average molecular weight of the epoxy monomer; M_C represents the average molecular weight of carbon atoms (12 g·mol⁻¹). The

results are listed in Table 1, from which it can be observed that the grafting densities of EFGO samples are in the range of 0.60 ~ 1.10%. Specifically, AFGO and AGGO show the highest and lowest grafting density, respectively. The phenomenon can be explained by the geometric effect. It is much easier for AFG90 molecule with the smallest molecular weight to enter into the GO interlayers and react with oxygen-containing groups on GO surfaces, and the process becomes more difficult for AG80 molecule with the highest molecular weight.

The grafting of epoxy monomers on GO surfaces also brings about significant structural changes, as evidenced by XRD spectra in Fig. 1c, d. GO sample shows a strong peak of 2theta at 11.2°, which corresponds to an interlayer distance of 0.79 nm according to Bragg's diffraction law. Comparatively, EFGO

Table 1 The grafting weight percent and grafting density of three EFGO samples

Samples	Grafting weight percent (G_W /wt%)	Grafting density (G_D /%)
EGO	19.82	0.76
AFGO	19.83	1.07
AGGO	18.50	0.65

samples all have enlarged interlayer distances due to the functionalization. EGO, AFGO and AGGO samples exhibit the peaks of 2θ at 10.15° , 8.32° and 7.15° , and the corresponding interlayer distances are 0.87 nm, 1.06 nm and 1.23 nm, respectively. The notably improved interlayer distances of EFGO samples indicate that epoxy chains are successfully grafted between EFGO sheets and are vital for EFGO sheets to exfoliate in epoxy matrix. In addition, the appearance of a new broad peak at 20.8° with an interlayer distance of 0.43 nm in the spectra of EFGO samples suggests the partial reduction and short-range restacking of GO during the functionalization [47].

Importantly, the interlayer distance of EFGO samples increases with the functionality degree of epoxy monomers. Actually, Yan et al. have reported that GO functionalized by poly(oxypropylene)amine with longer molecular chain length shows a larger interlayer distance [48]. It is suggested that the geometry characteristics and spatial configurations of the grafted chains between the layers play an important role in determining the interlayer distance of modified GO, by virtue of which the results in this work can be explained. Epoxy molecules with higher functionality degrees are more branched between GO sheets and tend to occupy a larger space. Therefore, it is easier for the tetrafunctional AG80 molecules to stretch around between EFGO sheets and effectively expand the interlayer distance, while the bifunctional E51 molecules tend to lie on the sheets and slightly enlarge the interlayer distance. The trifunctional AFG90 molecules are amid the two. It can also be anticipated that AGGO sample with the largest interlayer distance can show the highest degree of exfoliation in the matrix and be the most promising filler in reinforcing epoxy resin.

Raman spectra were utilized to reveal the structural integrity of EFGO samples, as shown in Fig. 1e. Two peaks of D band (1345 cm^{-1}) and G band (1585 cm^{-1}) in the spectra are attributed to the phonon breathing vibrations of sp^3 -hybridized carbon and sp^2 -hybridized carbon, respectively [49]. The

relative intensity ratio of D band against G band (I_D/I_G) is widely employed to evaluate the structural disorder degree of carbon materials [26, 44], as shown in Fig. 1f. The I_D/I_G value increases from 1.00 of GO to 1.02 of EGO, $1.16 \sim 1.18$ of AFGO and AGGO. This implies that EFGO samples have lower structural integrity due to the functionalization.

The morphologies of EFGO samples were revealed by AFM and SEM techniques, as shown in Fig. 2. EFGO samples are all in good sheet morphology with the sheet thickness ranging from 1.2 nm to 1.8 nm, which is similar to the reported results [24], indicating that EFGO samples are in a few layers. SEM images confirm that three EFGO samples are all flat sheets with some wrinkles and that the semitransparent sheets imply the improved exfoliation of EFGO samples.

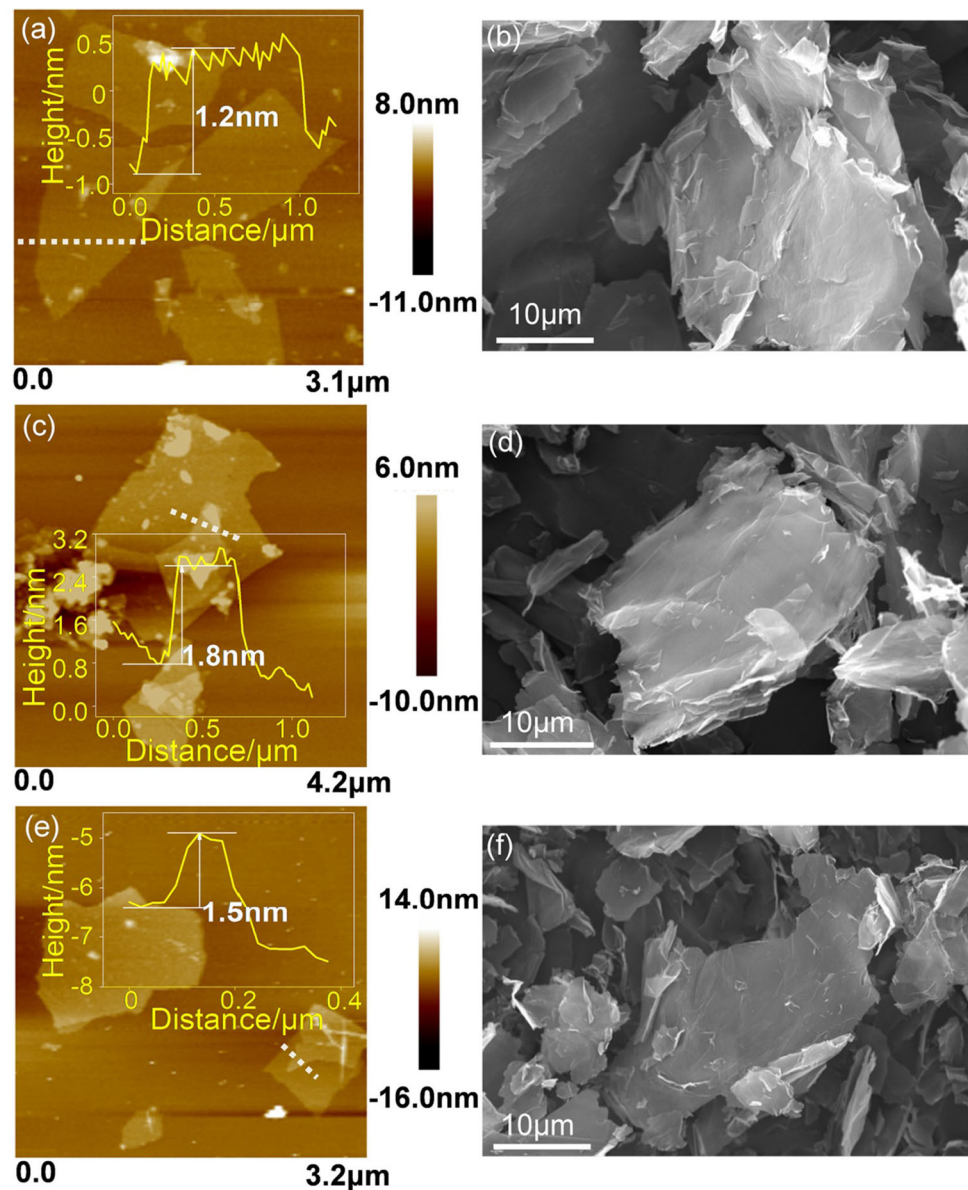
The high-resolution TEM images also provide detailed information for the morphology of EFGO samples, as presented in Fig. 3. It can be observed that all the EFGO samples show the similar transparent sheet morphology with some wrinkles on the surfaces. It seems that different species of epoxy monomers has not made significant alterations to the morphology of EFGO samples. Compared to GO, the edges of EFGO sheets become more obscure, which may be attributed to the chemical grafting of epoxy monomers on the surfaces.

Dispersion of epoxy-functionalized GO

As discussed in Supporting Information S4, the viscosity and rheological properties of EFGO/epoxy masterbatches show no obvious differences with those of neat epoxy; therefore, it is suggested that the introduction of EFGO fillers has not caused a great influence on the processing of the nanocomposites.

The dispersion of EFGO samples in epoxy matrix was investigated by optical microscope technique. As shown in Fig. S5, the number of large aggregates in the matrix before three-roll milling is reduced to a large extent after three-roll milling, suggesting the prominently enhanced dispersion state of EFGO.

Figure 2 AFM images of EGO (a), AFGO (c) and AGGO (e) with the inset images showing the thickness profile of the sheet as pointed out by the white line; SEM images of EGO (b), AFGO (d) and AGGO (f).



However, there are still some small visible aggregates in the matrix. The number of small aggregates is decreased for AFGO/epoxy masterbatch in comparison with EGO/epoxy masterbatch, and there are almost no aggregates in the AGGO/epoxy masterbatch.

XRD technique is widely used to reveal the exfoliation and dispersion state of GO and its derivatives in the nanocomposites [50, 51]. The diffraction peak of EFGO sheets in the nanocomposites reflects the exfoliated, intercalated or stacked state of the sheets, which is similar to that of two-dimensional clay [52]. As shown in Fig. 4, apart from the wide peak caused by the diffraction of neat epoxy, 0.30 wt% EGO/

epoxy and AFGO/epoxy nanocomposites show another small peak at 28.8° . The peak is attributed to the planar diffraction of EFGO sheets [53, 54], which is nonexistent in 0.30 wt% AGGO/epoxy nanocomposites. This implies that EFGO and AFGO sheets are in stacked or intercalated state in epoxy matrix with nonnegligible aggregation, while AGGO sheets show good exfoliation with little aggregation. However, the good exfoliation and dispersion of AGGO in the nanocomposites are impeded by the increased loading. At 0.50 wt% AGGO loading, the presence of the small diffraction peak at 28.8° implies the deteriorated exfoliation and dispersion state of AGGO sheets in the matrix.

Figure 3 TEM images of EGO (a), AFGO (b), AGGO (c) and GO (d).

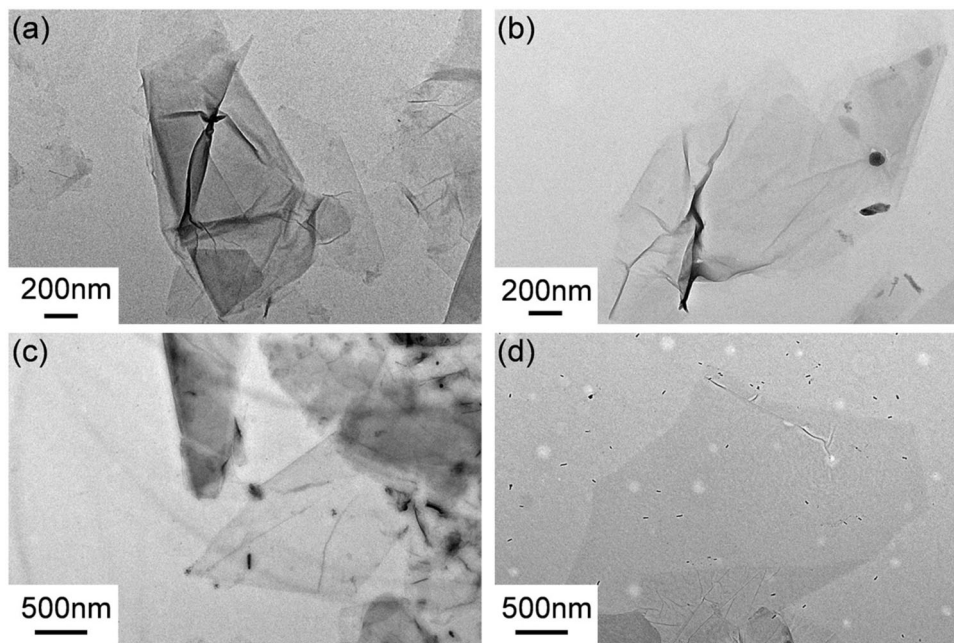
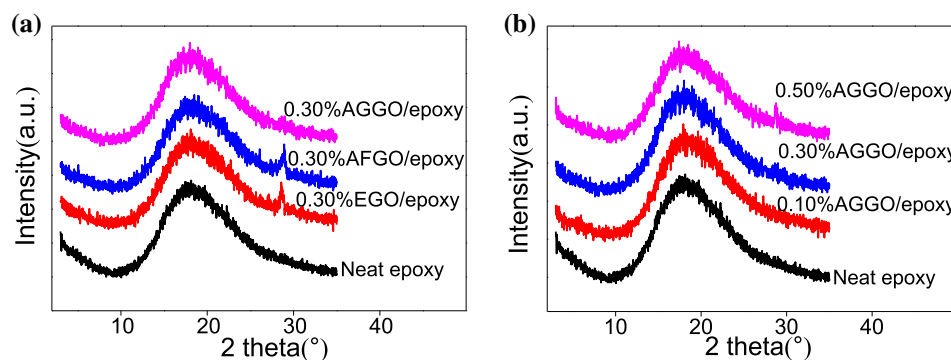


Figure 4 XRD spectra of neat epoxy and nanocomposites with 0.30 wt% EFGO (a), XRD spectra of neat epoxy and nanocomposites with different AGGO loadings (b).



TEM images provide more detailed information about the dispersion and interfacial characteristics of the nanocomposites, as presented in Fig. 5. As illustrated by the gray triangles, yellow squares and red circles, the black stacked bundles, the black loose lines and the hazy fuzzy gobbets are regarded as the aggregated, intercalated (or partly exfoliated) and exfoliated EFGO sheets according to the exfoliation degree of EFGO sheet. The similar phenomenon has also been reported in the functionalized GO/poly(ethylene glycol) and functionalized GO/polypropylene nanocomposites [55, 56]. Evidently, in 0.30 wt% EGO/epoxy nanocomposites and 0.30 wt% AFGO/epoxy nanocomposites, EFGO sheets are mainly in aggregation with little intercalation and exfoliation. Comparatively, AGGO sheets are in good intercalation and exfoliation state with little aggregation in the nanocomposites at 0.30 wt% or 0.10 wt% loading. The

greatly improved exfoliation and dispersion of AGGO sheets in the nanocomposites are attributed to their enlarged interlayer distance caused by the grafted AG80 molecules.

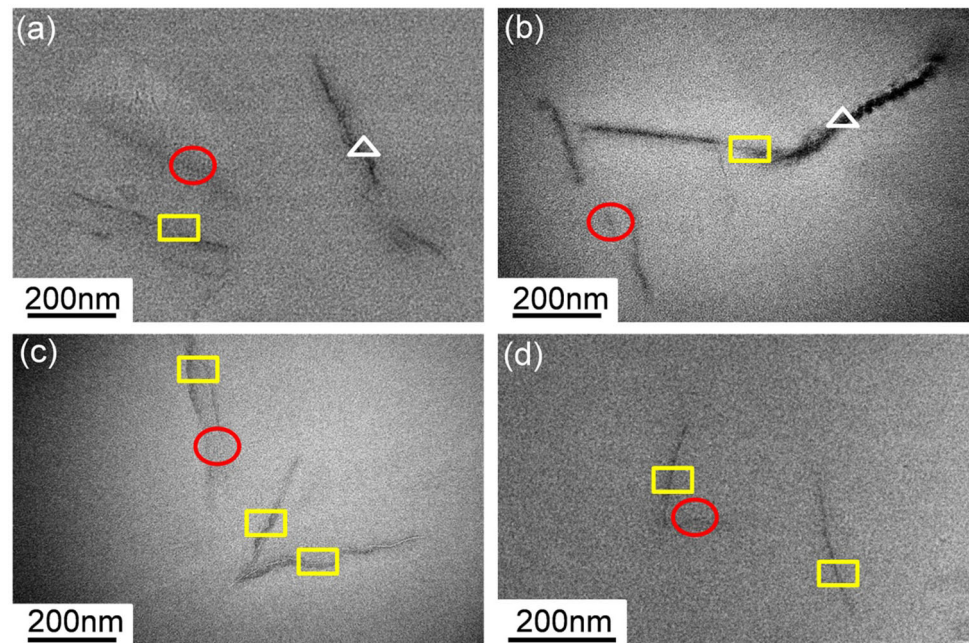
Mechanical properties of nanocomposites

Tensile properties at RT and LNT

The tensile properties of epoxy nanocomposites with EFGO loading ranging from 0.10 wt% to 0.50 wt% at RT and LNT were comprehensively investigated, and the results are shown in Fig. 6.

Basically, EFGO loading has an important influence on the mechanical properties of nanocomposites at both RT and LNT. The tensile strength and elongation at break of all the EFGO/epoxy nanocomposites reach the maximum value with no more than

Figure 5 The TEM images of 0.30 wt% EGO/epoxy nanocomposites (a), 0.30 wt% AFGO/epoxy nanocomposites (b), 0.30 wt% AGGO/epoxy nanocomposites (c) and 0.10 wt% AGGO/epoxy nanocomposites (d) with the gray \triangle , yellow \square and red \circ denoting the aggregated, intercalated and exfoliated EFGO sheets, respectively.



0.30 wt% EFGO and show a notable decrease at a loading of 0.50 wt%. It can be observed that the EFGO loadings at which the nanocomposites begin to show a decrease in tensile properties are not all the same for different EFGO samples at different temperatures of RT and LNT. The phenomenon has also been reported in previous researches [37, 57, 58], and the difference may be related to some accidental errors of experiments. Therefore, it is considered acceptable that there appear some fluctuations of the optimum loadings for different nanocomposite systems. At 0.50 wt% loading, the mechanical properties of nanocomposites are deteriorated to a large extent due to the easily formed aggregation of EFGO sheets in the matrix, as discussed in XRD results. The tensile modulus of the nanocomposites increases with the EFGO loading. The addition of EFGO with much higher modulus compared to epoxy resin enhances the modulus of the whole nanocomposites, and the trend follows the rule of mixtures of composite [59].

The maximum tensile properties of EFGO/epoxy nanocomposites are reliable and are believed to be the suitable representative parameters when comparing the reinforcing and toughening efficiency of three EFGO samples. Therefore, the maximum tensile properties of nanocomposites are mainly used in the discussion. At RT, the three EFGO samples are all effective reinforcement fillers when they are at appropriate loadings in the nanocomposites. To be

specific, 0.30 wt% EGO/epoxy nanocomposites, 0.30 wt% AFGO/epoxy nanocomposites and 0.10 wt% AGGO/epoxy nanocomposites show the maximum tensile strength of 67.1 MPa, 69.6 MPa and 73.1 MPa, which are 13.0%, 17.2% and 23.1% higher than that of neat epoxy. Meanwhile, the maximum elongation at break of the three nanocomposites can reach 10.5%, 10.8% and 12.3%, respectively, which are 1.0%, 3.8% and 18.3% higher than that of neat epoxy. The improved mechanical properties of EFGO/epoxy nanocomposites are attributed to the enhanced interfacial interactions between three EFGO samples and epoxy resin, which can also be supported by the thermomechanical properties, as discussed in Supporting Information S6.

What's important, the species of epoxy monomers grafted on EFGO surfaces also plays a vital role in the mechanical properties of epoxy nanocomposites. AGGO with the best exfoliation and dispersion state shows the highest efficiency in improving the tensile strength and elongation at break of epoxy resin, and EGO with the least satisfactory exfoliation and dispersion can only increase the tensile properties of epoxy resin to a limited extent. The efficiency of AFGO is amid the two due to its intermediate exfoliation and dispersion state. It can be concluded that the reinforcing efficiency of EFGO samples follows a trend of AGGO > AFGO > EGO, which is highly

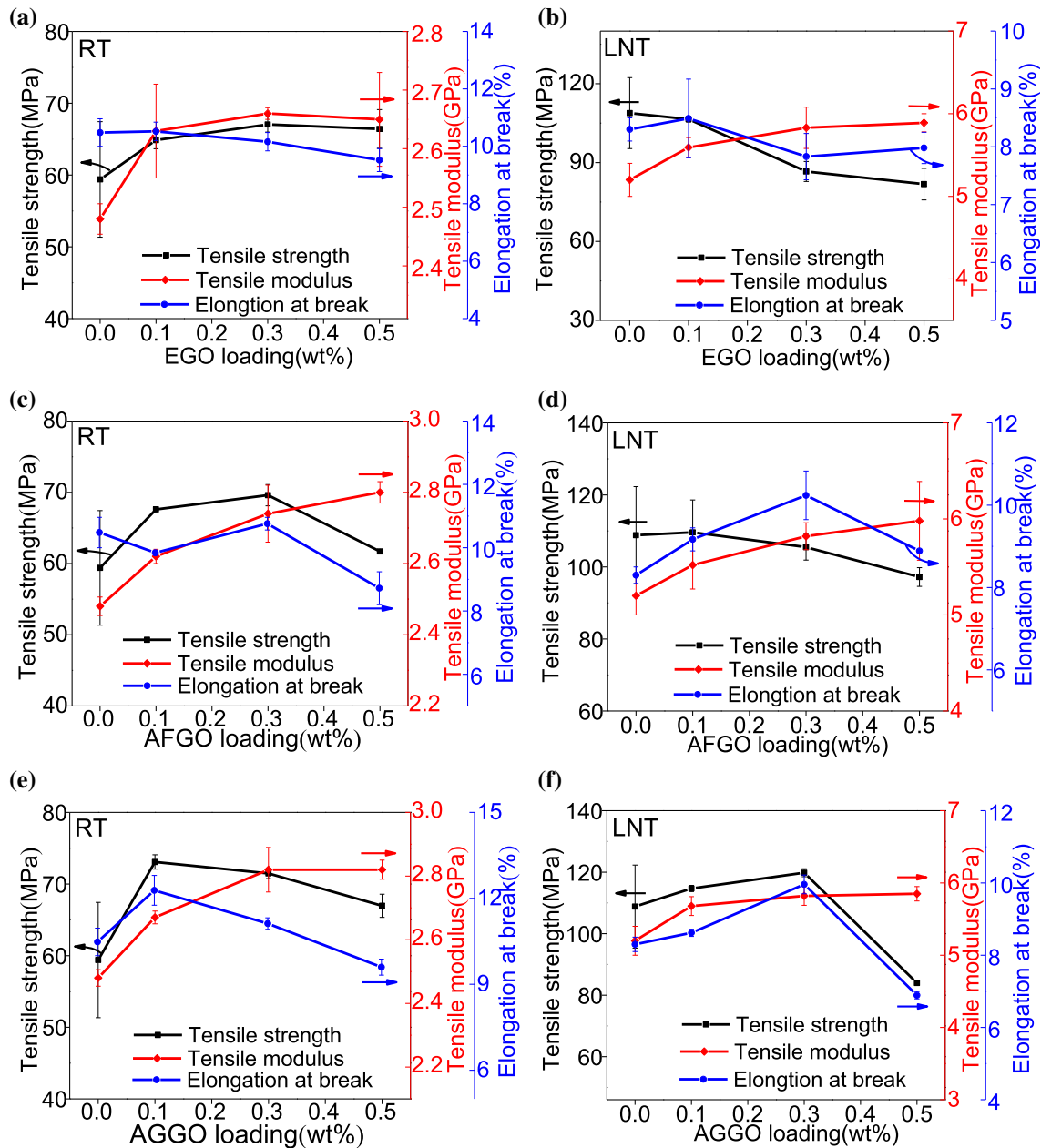


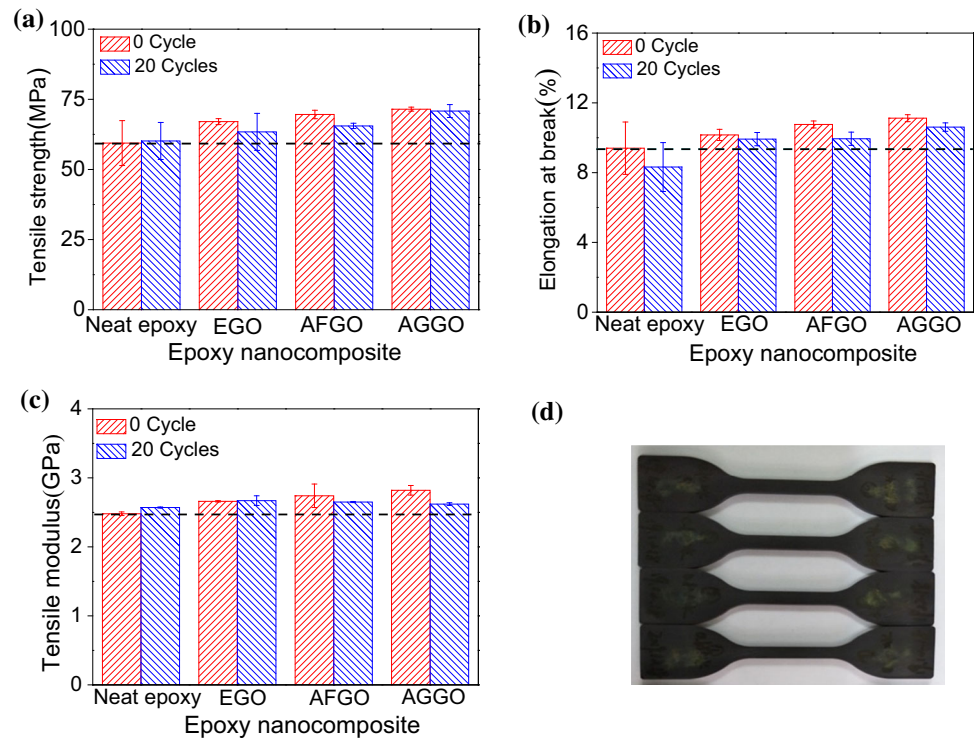
Figure 6 The tensile properties of EGO/epoxy nanocomposites at RT (a) and LNT (b), AFGO/epoxy nanocomposites at RT (c) and LNT (d), AGGO/epoxy nanocomposites at RT (e) and LNT (f) as a function of the loading.

consistent with the change of their exfoliation and dispersion state.

In comparison, the mechanical properties of nanocomposites at LNT show some differences. The prominent enhancement in the mechanical properties of nanocomposites exerted by EGO and AFGO at RT is rather weakened at LNT. Specifically, neat epoxy presents the tensile strength of 108.8 MPa and elongation at break of 8.30% at LNT. EGO/epoxy

nanocomposites with 0.10 wt% EGO show the maximum tensile strength of 106.5 MPa and the maximum elongation at break of 8.49%, indicating no advantage over neat epoxy. AFGO/epoxy nanocomposites with 0.30 wt% AFGO show the maximum tensile strength of 109.6 MPa and the maximum elongation at break of 10.24% at LNT, which are higher than that of neat epoxy to a small extent. The phenomenon can be explained that tensile samples

Figure 7 Tensile strength (a), elongation at break (b) and tensile modulus (c) of nanocomposites with 0.30 wt% EFGO before and after thermal cycling and the image of tensile samples after thermal cycling (d).



are more sensitive to defects like aggregation of EFGO sheets at LNT than at RT, which is similar to the research results of Reed et al. that the sensitivity of tensile strength to flaws of epoxy resins at low temperature (76–4 K) was about twice the room-temperature sensitivity [60]. In the case of AGGO/epoxy nanocomposites, the good exfoliation and dispersion of AGGO sheets make an important contribution to the greatly improved mechanical properties at LNT. With 0.30 wt% AGGO, the nanocomposites exhibit the maximum tensile strength of 119.8 MPa and the highest elongation at break of 9.96%, which are 10.1% and 20.0% higher than that of neat epoxy at LNT, respectively.

Furthermore, the tensile fracture energy calculated from the integration of the stress–strain curve is also utilized to evaluate the fracture toughness of the nanocomposites and the results are listed in Table S3. All the nanocomposites exhibit the highest tensile toughness with 0.10–0.30 wt% EFGO. As the loading increases further, the toughness of nanocomposites is decreased. The three EFGO/epoxy nanocomposites exhibit enhanced toughness to varying degrees compared to neat epoxy at both RT and LNT. The maximum increase is attained by 0.30 wt% AGGO/

epoxy nanocomposites which achieve the improvement of 9.0% and 25.5% at RT and LNT, respectively.

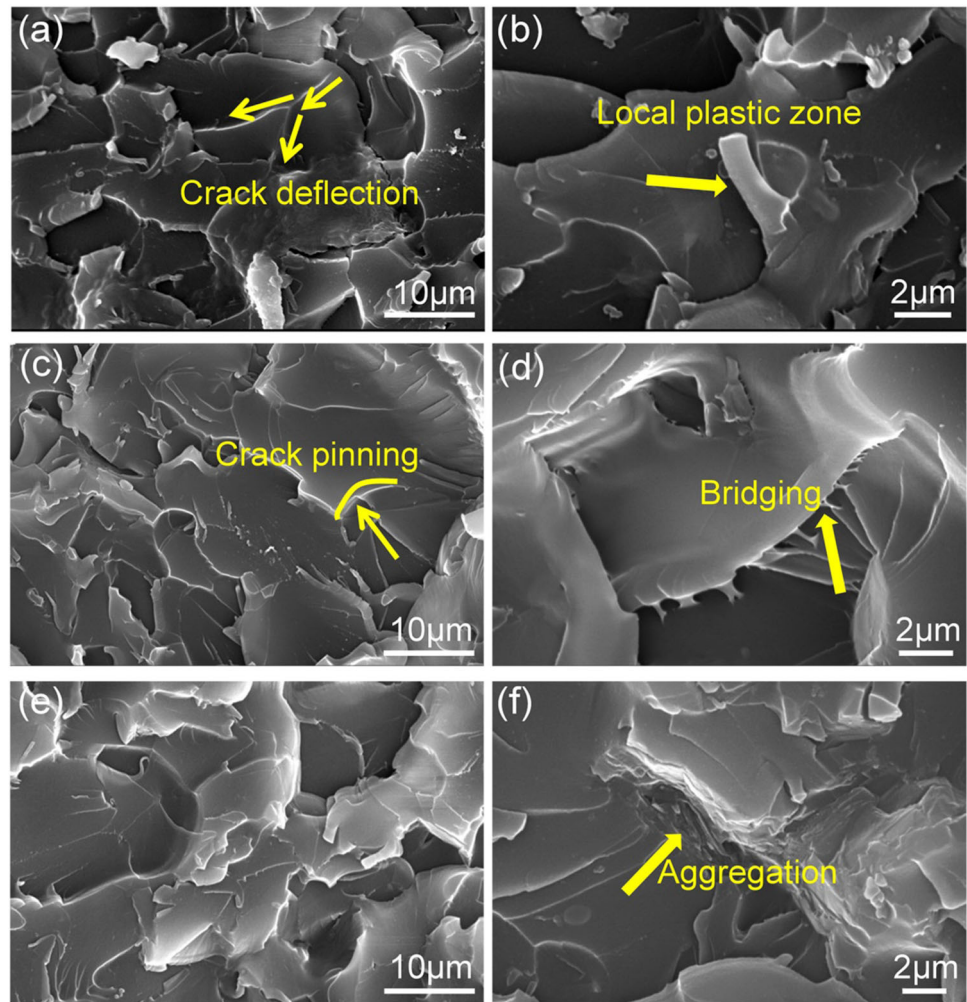
It can be concluded that among three EFGO samples, AGGO exhibits the highest efficiency in strengthening and toughening epoxy resin at both RT and LNT. The change in the mechanical properties of nanocomposites agrees well with the exfoliation and dispersion state of EFGO samples. The superior exfoliation and dispersion of AGGO sheets in the matrix owing to the enlarged interlayer distance caused by the grafted AG80 molecules lead to the outstanding mechanical performance of the nanocomposites.

Tensile properties after thermal cycling

Tensile tests were performed on samples after thermal cycling to qualitatively evaluate the influence of thermal cycling on the mechanical properties of neat epoxy and nanocomposites. The results are shown in Fig. 7.

The change extents of the mechanical properties of neat epoxy and nanocomposites with 0.3 wt% EFGO after thermal cycling are listed in Table S4. It can be found that neat epoxy and all the nanocomposites show no prominent changes in the tensile strength

Figure 8 SEM images of the tensile fractured surfaces of nanocomposites at LNT with 0.10 wt% EGO (a), 0.10 wt% AFGO (c) and 0.10 wt% AGGO (e), and the enlarged area of local plastic deformation zone (b), local interfacial bridging (d) and local aggregated EGO sheets (f).



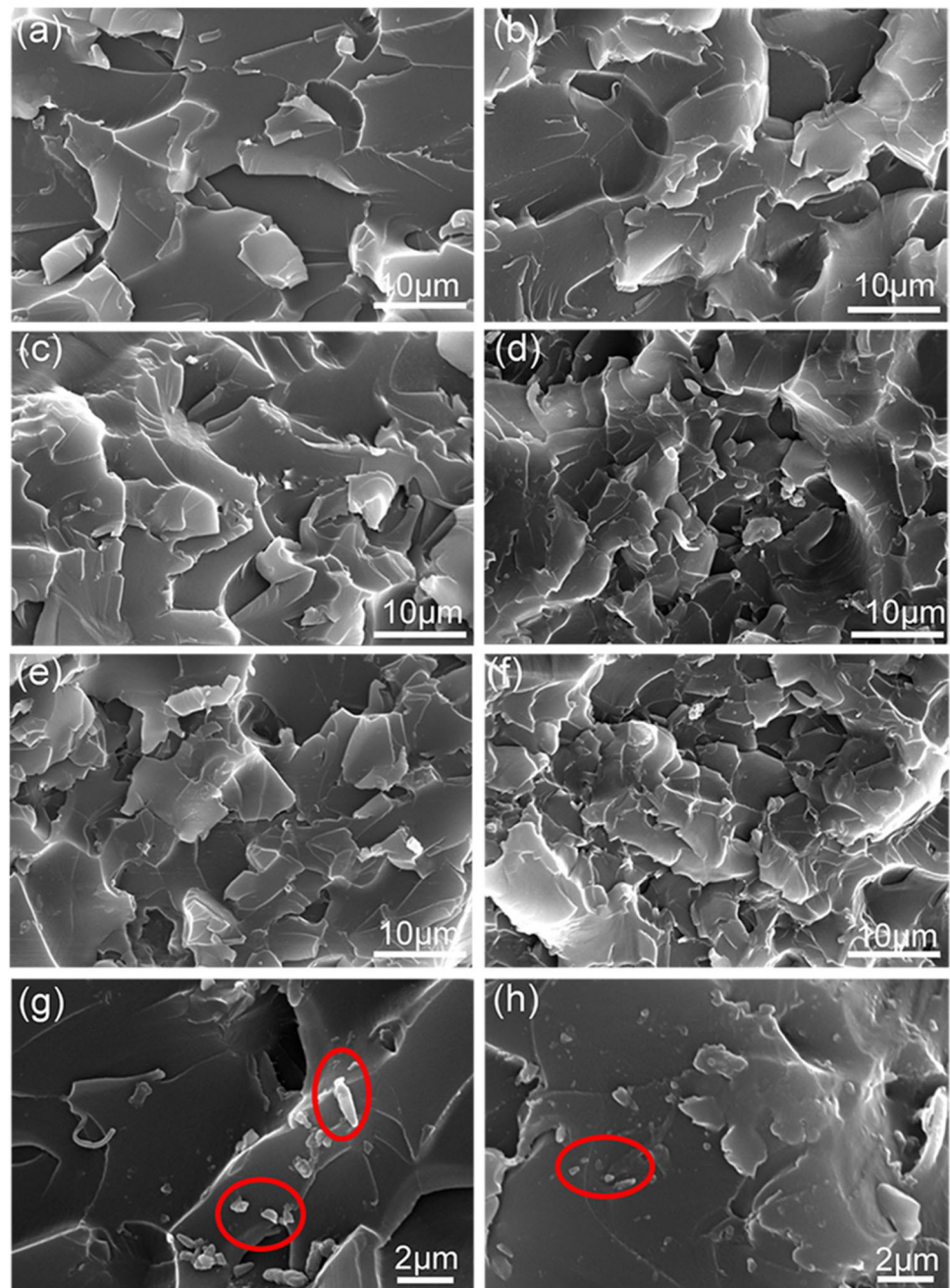
and tensile modulus. The most important change lies in the decrease of the elongation at break which ranges from 1 to 21%. Compared to neat epoxy, nanocomposites show a smaller decrease in elongation at break. The decrease in the tensile properties of nanocomposites is attributed to the accumulated internal thermal stress during thermal cycling, which induces the occurrence of cracks and results in the decreased tensile properties.

On the whole, all the nanocomposites present higher tensile strength and elongation at break than neat epoxy after thermal cycling. Especially, AGGO/epoxy nanocomposites show the tensile strength of 70.8 MPa and the elongation at break of 10.6%, which are 17.8% and 27.7% higher than those of neat epoxy, respectively. The results demonstrate that surface functionalization of GO by epoxy monomers is effective in improving the resistance of nanocomposites to the thermal cycling.

Fracture morphology and toughening mechanisms

The tensile fractured surfaces of the nanocomposites were studied to reveal the interfacial characteristics and toughening mechanisms of EFGO sheets at RT and LNT. It can be observed from Fig. S7 that neat epoxy exhibits the typical feature of brittle fracture at both RT and LNT as illustrated by the smooth fractured surfaces with river-like patterns [61]. The introduction of EFGO sheets makes a great change to the fracture morphology of nanocomposites. There appear large numbers of tortuous cracks and tear ridges, implying that EFGO sheets can change the crack propagation direction and extend the crack path, as shown in Fig. 8a. Also, the cracks can be pinned by the two-dimensional EFGO sheets, leading to more energy consumption, as presented in Fig. 8c. Therefore, crack deflection and crack pinning are two

Figure 9 SEM images of the tensile fractured surfaces of nanocomposites with 0.10 wt% AGGO (a), 0.30 wt% AGGO (c) and 0.50 wt% AGGO (e) at RT and with 0.10 wt% AGGO (b), 0.30 wt% AGGO (d) and 0.50 wt% AGGO (f) at LNT; the enlarged image of the pullout of AGGO sheets at LNT (g, h).



prominent toughening mechanisms of EFGO sheets in the nanocomposites [62].

Besides, large numbers of deformed branches can be seen in the fractured surfaces of nanocomposites at LNT, as presented in Fig. 8b. These branches are local plastic zones formed in the tensile tests, suggesting that significant plastic deformation occurs at the crack tip during the fracture process. Interestingly, there is a special phenomenon that some interfacial bridging which connects the two adjacent broken

interfaces in the different planes is developed, as shown in Fig. 8d. The bridging is probably related to the strong covalent bonds formed between EFGO sheets and epoxy matrix, contributing to the much stronger stress transfer from the matrix to EFGO sheets. Moreover, some aggregated EFGO sheets can also be observed in the fractured surfaces, as shown in Fig. 8f, and the aggregation may become the stress concentration location and induce the crack.

The fractured surfaces of AGGO/epoxy nanocomposites with different AGGO loadings at RT and LNT are also compared, as shown in Fig. 9. The fracture morphology at LNT is basically similar to that at RT. However, the fractured surfaces of nanocomposites at LNT are covered with some small fragments as presented in Fig. 9 (g-h). This means that the pullout of EFGO sheets from the matrix also plays a role in toughening the matrix. The phenomenon is related to the mismatch between the thermal expansion coefficients of the matrix and EFGO sheets under cryogenic conditions [36, 63]. What's more, as AGGO loading increases, the tear ridges in the fractured surfaces become smaller and the sidestep-shaped patterns become denser. It can be explained that the increased number of AGGO sheets causes the intensified separation of matrix between EFGO sheets.

In addition, the thermal properties of the nanocomposites were also investigated, showing slight change compared to that of neat epoxy. The results are carefully discussed in Supporting Information S10.

Conclusions

In this work, three epoxy-functionalized GO samples (EGO, AFGO, AGGO) were successfully prepared and characterized by FTIR, TG, XRD, Raman, AFM and SEM techniques. The interlayer distance of EFGO samples increases with the functionality degree of the grafted epoxy monomers and AGGO exhibits the largest interlayer distance. All the EFGO/epoxy nanocomposites reach the maximum tensile properties with no more than 0.30 wt% EFGO and show a great decrease at a higher loading of 0.50 wt%. At appropriate EFGO loadings, nanocomposites all show improved mechanical properties compared to neat epoxy, indicating the strengthened interfacial interactions between EFGO and epoxy resin. The enhancement of the mechanical properties follows a trend of AGGO > AFGO > EGO-modified nanocomposites, which is highly consistent with the change of the exfoliation and dispersion state of EFGO sheets in the matrix. AGGO with the largest interlayer distance shows the best exfoliation and dispersion in the matrix, contributing to the highest mechanical properties of corresponding nanocomposites at RT, LNT and after thermal cycling. Crack

deflection, crack pinning and interfacial bridging are all active toughening mechanisms of EFGO at both RT and LNT. The pullout of EFGO sheets from the matrix is another toughening mechanism at LNT. This work is believed to provide a new insight into the design of surface-functionalized GO and high-performance nanocomposites applied in the cryogenic environment.

Acknowledgements

This work was financially supported by the National Natural Science Foundation of China (51773006).

Declarations

Conflicts of interest The authors declare that they have no conflicts of interest.

Supplementary Information: The online version contains supplementary material available at <http://doi.org/10.1007/s10853-021-06580-z>.

References

- [1] Lee C, Wei X, Kysar JW, Hone J (2008) Measurement of the elastic properties and intrinsic strength of monolayer graphene. *Science* 321:385–388
- [2] Balandin AA, Ghosh S, Bao W, Calizo I, Teweldebrhan D, Miao F, Lau CN (2008) Superior thermal conductivity of single-layer graphene. *Nano Lett* 8(3):902–907
- [3] Bolotin KI, Sikes KJ, Jiang Z, Klima M, Fudenberg G, Hone J, Kim P, Stormer HL (2008) Ultrahigh electron mobility in suspended graphene. *Solid State Commun* 146:351–355
- [4] Ma W, Li W, Li M, Mao Q, Pan Z, Zhu M, Zhang Y (2020) Scalable microgel spinning of a three-dimensional porous graphene fiber for high-performance flexible supercapacitors. *J Mater Chem A* 8:25355–25362
- [5] Rostami S, Puza F, Ucak M, Ozgur E, Gul O, Ercan UK, Garipcan B (2021) Bifunctional sharkskin mimicked chitosan/graphene oxide membranes: reduced biofilm formation and improved cytocompatibility. *Appl Surf Sci* 544:148828
- [6] Jen YM, Chang HH, Lu CM, Liang SY (2021) Temperature-dependent synergistic effect of multi-walled carbon nanotubes and graphene nanoplatelets on the tensile quasi-static and fatigue properties of epoxy nanocomposites. *Polymers* 13:84

- [7] Rafiee MA, Rafiee J, Wang Z, Song H, Yu ZZ, Koratkar N (2009) Enhanced mechanical properties of nanocomposites at low graphene content. *ACS Nano* 3(12):3884–3890
- [8] Hadaeghnia M, Ahmadi S, Ghasemi I, Wood-Adams PM (2020) Manipulating the morphology of PA6/POE blends using graphene to achieve balanced electrical and mechanical properties. *Compos Sci Technol* 200:108412
- [9] Klimchitskaya GL, Mostepanenko M (2013) Van der Waals and Casimir interactions between two graphene sheets. *Phys Rev B* 87:1081–1089
- [10] Fu Y, Liu L, Zhang JW, Hiscox WC (2014) Functionalized graphenes with polymer toughener as novel interface modifier for property-tailored polylactic acid/graphene nanocomposites. *Polymer* 55:6381–6389
- [11] Prusty RK, Rathore DK, Sahoo S, Parida V, Ray BC (2017) Mechanical behaviour of graphene oxide embedded epoxy nanocomposite at sub- and above- zero temperature environments. *Compos Commun* 3:47–50
- [12] Cui J, Shan W, Xu J, Qiu H, Li J, Yang J (2020) Effect of silane-bridging on the dispersion of polyetheramine-functionalized graphene oxide in waterborne epoxy composites. *Compos Sci Technol* 200:108438
- [13] Zhang F, Liu W, Liang L, Yang M, Wang S, Shi H, Xie Y, Pi K (2020) Application of polyether amine intercalated graphene oxide as filler for enhancing hydrophobicity, thermal stability, mechanical and anti-corrosion properties of waterborne polyurethane. *Diam Relat Mater* 109:108077
- [14] Xie Y, Liu W, Liu C, He S, Zhang F, Shi H, Yang M, Wang Z (2019) Investigation of covalently grafted polyacrylate chains onto graphene oxide for epoxy composites with reinforced mechanical performance. *J Appl Polym Sci* 136(32):47842
- [15] Rahman SS, Arshad M, Zubair M, Ghasri-Khouzani M, Qureshi A, Ullah A (2020) Facile fabrication of graphene oxide/poly(styrene-co-methyl methacrylate) nanocomposite with high toughness and thermal stability. *Mater Today Commun* 25:101633
- [16] Li T, Meng Z, Ketten S (2020) Interfacial mechanics and viscoelastic properties of patchy graphene oxide reinforced nanocomposites. *Carbon* 158:303–313
- [17] Hussein A, Sarkar S, Oh D, Lee K, Kim B (2016) Epoxy/p-phenylenediamine functionalized graphene oxide composites and evaluation of their fracture toughness and tensile properties. *J Appl Polym Sci* 133(34):43821
- [18] Niu M, Wang H, Li J, Chen H, Li L, Yang H, Liu X, Chen Z, Liu H, Chen J (2020) Polyethylene glycol grafted with carboxylated graphene oxide as a novel interface modifier for polylactic acid/graphene nanocomposites. *Roy Soc Open Sci* 7:192154
- [19] Seong M, Kim DS (2015) Effects of facile amine-functionalization on the physical properties of epoxy/graphene nanoplatelets nanocomposites. *J Appl Polym Sci* 132(28):42269
- [20] Feng P, Song G, Li X, Xu H, Xu L, Lv D, Zhu X, Huang Y, Ma L (2021) Effects of different “rigid-flexible” structures of carbon fibers surface on the interfacial microstructure and mechanical properties of carbon fiber/epoxy resin composites. *J Colloid Interf Sci* 583:13–23
- [21] Kadhim N, Zaman A, Jiang M, Li Y, Yang X, Qiu J, Zhou Z (2021) A cast-in-place fabrication of high performance epoxy composites cured in an in-situ synthesized 3D foam of nanofibers. *Compos Part B-Eng* 205:108495
- [22] Jyotishkumar P, Moldenaers P, George SM, Thomas S (2012) Viscoelastic effects in thermoplastic poly(styrene-acrylonitrile)-modified epoxy-DDM system during reaction induced phase separation. *Soft Matter* 8(28):7452–7462
- [23] Jyotishkumar P, Özdilek C, Moldenaers P, Sinturel C, Janke A, Pionteck J, Thomas S (2010) Dynamics of phase separation in poly(acrylonitrile-butadiene-styrene)-modified epoxy/DDS system: kinetics and viscoelastic effects. *J Phys Chem B* 114(42):13271–13281
- [24] Wang X, Li N, Wang J, Li G, Zong L, Liu C, Jian X (2018) Hyperbranched polyether epoxy grafted graphene oxide for benzoxazine composites: enhancement of mechanical and thermal properties. *Compos Sci Technol* 155:11–21
- [25] Shen B, Zhai W, Tao M, Lu D, Zheng W (2013) Chemical functionalization of graphene oxide toward the tailoring of the interface in polymer composites. *Compos Sci Technol* 77:87–94
- [26] Wan YJ, Tang LC, Gong LX, Yan D, Li YB, Wu LB, Jiang JX, Lai GQ (2014) Grafting of epoxy chains onto graphene oxide for epoxy composites with improved mechanical and thermal properties. *Carbon* 69:467–480
- [27] Guan LZ, Wan YJ, Gong LX, Yan D, Tang LC, Wu LB, Jiang JX, Lai GQ (2014) Toward effective and tunable interphases in graphene oxide/epoxy composites by grafting different chain lengths of polyetheramine onto graphene oxide. *J Mater Chem A* 2(36):15058–15069
- [28] Huang C, Ren MF, Li T, Chang X, Cong J, Lei YJ (2016) Trans-scale modeling framework for failure analysis of cryogenic composite tanks. *Compos Part B- Eng* 85:41–49
- [29] Ma HL, Jia Z, Lau KT, Li X, Hui D, Shi SQ (2017) Enhancement on mechanical strength of adhesively-bonded composite lap joints at cryogenic environment using coiled carbon nanotubes. *Compos Part B-Eng* 110:396–401
- [30] Li H, Wang K, Chen G, Sun L, Yang J (2020) Internal stress analysis of epoxy adhesively-boned joints based on their thermomechanical properties at cryogenic temperature. *J Appl Polym Sci* 137:49311

- [31] Rosetti Y, Alcouffé P, Pascault JP, Gerard JF, Lortie F (2018) Polyether sulfone-based epoxy toughening: from micro- to nano-phase separation via PES end-chain modification and process engineering. *Materials* 11(10):1960
- [32] Rodríguez ES, Falchi VG, Asaro L, Zucchi IA, Williams RJJ (2019) Toughening an epoxy network by the addition of an acrylic triblock copolymer and halloysite nanotubes. *Compos Commun* 12:86–90
- [33] Surendran A, Pionteck J, Vogel R, Kalarikkal N, Geethamma GV, Thomas S (2018) Effect of organically modified clay on the morphology, rheology and viscoelasticity of epoxy-thermoplastic nanocomposites. *Polym Test* 70:18–29
- [34] Tian J, Yang J, Yang C, Hao S (2019) Compression and reduction of graphene oxide aerogels into flexible, porous and functional graphene films. *J Mater Sci* 54:13147–13156. <https://doi.org/10.1007/s10853-019-03828-7>
- [35] Tian J, Yang C, Yang J, Hao S (2021) The correlated effects of filler loading on the curing reaction and mechanical properties of graphene oxide reinforced epoxy nanocomposites. *J Mater Sci* 56:3723–3737
- [36] Fan J, Yang J, Li H, Tian J, Wang M, Zhao Y (2021) Cryogenic mechanical properties of graphene oxide/epoxy nanocomposites: influence of graphene oxide with different oxidation degrees. *Polym Test* 96:107074
- [37] Li H, Wang K, Chen G, Sun L, Yang J (2020) Cryogenic mechanical properties and failure mechanism of epoxy nanocomposites modified by multiwalled carbon nanotubes with tunable oxygen-containing groups on surface. *J Appl Polym Sci* 137:49266
- [38] Li J, Wu Z, Huang C, Huang R, Li L (2014) Mechanical behaviors of hyperbranched epoxy toughened bisphenol F epoxy resin for cryogenic applications. *AIP Conf Proc* 125:1574
- [39] Zhao Y, Chen ZK, Liu Y, Xiao HM, Feng QP, Fu SY (2013) Simultaneously enhanced cryogenic tensile strength and fracture toughness of epoxy resins by carboxylic nitrile-butadiene nano-rubber. *Compos Part A-Appl S* 55:178–187
- [40] Zhao H, Ding J, Yu H (2018) Variation of mechanical and thermal properties in sustainable graphene oxide/epoxy composites. *Sci Rep* 8:16560
- [41] Qi Z, Tan Y, Zhang Z, Gao L, Zhang C, Tian J (2018) Synergistic effect of functionalized graphene oxide and carbon nanotube hybrids on mechanical properties of epoxy composites. *RSC Adv* 8(67):38689–38700
- [42] Yu G, Wu P (2014) Effect of chemically modified graphene oxide on the phase separation behaviour and properties of an epoxy/polyetherimide binary system. *Polym Chem* 5:96–104
- [43] Li FY, Huang L, Li Q, Wang X, Ma XL, Jiang CN, Zhou XQ, Duan WG, Lei FH (2019) Synthesis and antiproliferative evaluation of novel hybrids of dehydroabiestic acid bearing 1,2,3-triazole moiety. *Molecules* 24:4191
- [44] Wei Y, Hu X, Jiang Q, Sun Z, Wang P, Qiu Y, Liu W (2018) Influence of graphene oxide with different oxidation levels on the properties of epoxy composites. *Compos Sci Technol* 161:74–84
- [45] Zhou H, Zhai HJ (2018) Boosting the electrochemical capacitive properties of polypyrrole using carboxylated graphene oxide as a new dopant. *J Mater Sci-Mater El* 29:7893–7903. <https://doi.org/10.1007/s10854-018-8789-6>
- [46] Fan J, Yang J, Wang L, Li H, Tian J, Ye J, Zhao Y (2021) Enhanced mechanical properties of epoxy nanocomposites with mildly surface-functionalized graphene oxide by tuned amine species. *Appl Surf Sci* 558:149964
- [47] Rohini R, Bose S (2018) Extraordinary improvement in mechanical properties and absorption-driven microwave shielding through epoxy-grafted graphene “interconnects.” *ACS Omega* 3(3):3200–3210
- [48] Yan L, Zhou Y, Zhang X, Zou H, Chen Y, Liang M (2019) Effect of graphene oxide with different exfoliation levels on the mechanical properties of epoxy nanocomposites. *Polym Bull* 76:6033–6047
- [49] Tian W, Gao Q, Tan Y, Yang K, Zhu L, Yang C, Zhang H (2015) Bio-inspired beehive-like hierarchical nanoporous carbon derived from bamboo-based industrial by-product as a high performance supercapacitor electrode material. *J Mater Chem A* 3:5656–5664
- [50] Zhang D, Fu L, Liao L, Liu N, Dai B, Zhang C (2012) Preparation, characterization, and application of electrochemically functional graphene nanocomposites by one-step liquid-phase exfoliation of natural flake graphite with methylene blue. *Nano Res* 5(12):875–887
- [51] Wang Z, Tang XZ, Yu ZZ, Guo P, Song HH, Du XS (2011) Dispersion of graphene oxide and its flame retardancy effect on epoxy nanocomposites. *Chinese J Polym Sci* 29(3):368–376
- [52] Rao Y, Pochan JM (2007) Mechanics of polymer-clay nanocomposites. *Macromolecules* 40(2):290–296
- [53] Okan BS (2017) Fabrication of multilayer graphene oxide-reinforced high density polyethylene nanocomposites with enhanced thermal and mechanical properties via thermokinetic mixing. *Turk J Chem* 41:381–390
- [54] Vuluga D, Thomassin JM, Molenberg I, Huynen I, Gilbert B, Jérôme C, Alexandre M, Detrembleur C (2011) Straight-forward synthesis of conductive graphene/polymer nanocomposites from graphite oxide. *Chem Commun* 47(9):2544–2546
- [55] Hu Y, Sun CB, Kou J (2020) Exfoliation of poly(ethylene glycol)-intercalated graphite oxide composite in water without sonication. *Int J Min Met Mater* 27(6):840–845

- [56] Chen X, Ma Y, Cheng Y, Zhang A, Liu W (2019) Enhanced mechanical and flame-resistant properties of polypropylene nanocomposites with reduced graphene oxide-functionalized ammonium polyphosphate and pentaerythritol. *J Appl Polym Sci* 136(41):48036
- [57] Park YT, Qian Y, Chan C, Suh T, Nejhad MG, Macosko CW, Stein A (2015) Epoxy toughening with low graphene loading. *Adv Funct Mater* 25(4):575–585
- [58] Jiang T, Kuila T, Kim NH, Ku BC, Lee JH (2013) Enhanced mechanical properties of silanized silica nanoparticle attached graphene oxide/epoxy composites. *Compos Sci Technol* 79(5):115–125
- [59] Tham MW, Fazita MN, Khalil HA, Zuhudi NZM, Jaafar M, Rizal S, Haafiz MM (2018) Tensile properties prediction of natural fibre composites using rule of mixtures: A review. *J Reinf Plast Comp* 38:211–248
- [60] Reed RP, Walsh RP (1994) Tensile properties of resins at low temperatures. *Adv Cryog Eng* 40:1129–1136
- [61] Olowojoba GB, Eslava S, Gutierrez ES, Kinloch AJ, Mattevi C, Rocha VG, Taylor AC (2016) In situ thermally reduced graphene oxide/epoxy composites: thermal and mechanical properties. *Appl Nanosci* 6:1015–1022
- [62] Hussein A, Sarkar S, Lee K, Kim B (2017) Cryogenic fracture behavior of epoxy reinforced by a novel graphene oxide/poly(p-phenylenediamine) hybrid. *Compos Part B-Eng* 129:133–142
- [63] Quaresimin M, Schulte K, Zappalorto M, Chandrasekaran S (2016) Toughening mechanisms in polymer nanocomposites: from experiments to modeling. *Compos Sci Technol* 123:187–204

Publisher's Note Springer Nature remains neutral with regard to jurisdictional claims in published maps and institutional affiliations.